BBA - Molecular Basis of Disease 1865 (2019) 2633–2646

Contents lists available at ScienceDirect

BBA - Molecular Basis of Disease

journal homepage: www.elsevier.com/locate/bbadis

The regulation of NDRG2 expression during ATLL development after HTLV-1 infection

Tomonaga Ichikawa[a], Shingo Nakahata[a], Masahiro Fujii[b], Hidekatsu Iha[c], Kazuya Shimoda[d], Kazuhiro Morishita[a,*]

[a] Division of Tumor and Cellular Biochemistry, Department of Medical Sciences, Faculty of Medicine, University of Miyazaki, 5200 Kihara, Kiyotake, Miyazaki 889-1692, Japan
[b] Division of Virology, Graduate School of Medical and Dental Sciences, Niigata University, Niigata 951-8510, Japan
[c] Department of Microbiology, Faculty of Medicine, Oita University, Yufu, Oita 879-5593, Japan
[d] Division of Gastroenterology and Hematology, Department of Internal Medicine, Faculty of Medicine, University of Miyazaki, 5200 Kihara, Kiyotake, Miyazaki 889-1692, Japan

ARTICLE INFO

Keywords:
NDRG2
EZH2
DNA promoter methylation
ATLL

ABSTRACT

N-myc downstream-regulated gene 2 (NDRG2) is a candidate tumor suppressor that is frequently downregulated in adult T-cell leukemia/lymphoma (ATLL) and functions to negatively regulate several cellular signaling pathways as PP2A recruiter. To clarify the molecular mechanisms of suppression of NDRG2 expression, we initially determined the expression pattern of NDRG2 in various types of T-cells and ATLL cells. NDRG2 expression was significantly upregulated in HTLV-1/Tax-immortalized T-cells, which was mediated by NF-κB activation through Tax expression. On the other hand, NDRG2 expression was suppressed in HTLV-1-infected cell lines and various types of ATLL cells, which was dependent on the DNA methylation of the NDRG2 promoter. We found that the expression of enhancer of zeste homolog 2 (EZH2), a member of the polycomb family, is increased in ATLL, and that EZH2 directly binds to the NDRG2 promoter and induces DNA methylation of the NDRG2 promoter. Since the expression of EZH2 were anti-parallelly regulated with the NDRG2 expression, EZH2 might be one of the most important regulators of the downregulation of NDRG2, contributing to enhanced activation of signaling pathways during ATLL development.

1. Introduction

Adult T-cell leukemia/lymphoma (ATLL) is an aggressive $CD4^+$ T-cell malignancy associated with human T-cell leukemia virus type 1 (HTLV-1) infection. HTLV-1 oncogenic proteins Tax and HBZ induce not only the aberrant activation of signal transduction pathways such as PI3K/AKT, MAPK, Jak/STAT, and NF-κB, but also the accumulation of abnormal genomic and epigenetic changes, leading to transformation and cell proliferation of HTLV-1-infected T-cells, and < 5% of HTLV-1 carriers finally develop ATLL after a long latency period of > 50 years [1,2]. Our previous studies demonstrated that the expression of a novel tumor suppressor gene, N-myc downstream-regulated gene 2 (NDRG2), is frequently downregulated in ATLL and many types of other cancers, and that the down-regulation of NDRG2 leads to activation of the PI3K/AKT and NF-κB signaling pathways through functional inactivation of PTEN via an enhancement of its phosphorylation [3–5]. Because NDRG2 promotes the dephosphorylation of PTEN via the recruitment of protein phosphatase 2A (PP2A) to PTEN, NDRG2 may play an important role in the regulation of several signaling transduction pathways through the recruitment of PP2A to signaling molecules other than PTEN. Because NDRG2 expression is upregulated by stress responses, such as genotoxic p53, hypoxic HIF1α, oxidative stress, and inflammation [6–11], NDRG2 may suppress stress-induced aberrant signal transduction pathways by promoting PP2A-dependent dephosphorylation of proteins. Therefore, it is of particularly importance to understand the detailed molecular mechanisms of the regulation of NDRG2 expression to elucidate the mechanism of tumorigenesis in ATLL and other cancers.

Tumor suppressor genes are often downregulated through aberrant genomic and epigenetic modifications, which are associated with tumor development. In addition to genomic alterations such as mutations and deletions, the aberrant DNA hypermethylation of CpG islands in the promoter region and histone modifications are widely observed in many types of cancers and are related to the silencing of transcription of

* Corresponding author.
E-mail address: kmorishi@med.miyazaki-u.ac.jp (K. Morishita).

https://doi.org/10.1016/j.bbadis.2019.07.001
Received 15 March 2019; Received in revised form 25 June 2019; Accepted 4 July 2019
Available online 08 July 2019

tumor suppressor genes in a tumor-type specific manner [12,13]. The expression of adenomatous polyposis (APC), p16 (CDKN2A), Kruppel-like factor 4 (KLF4), human post-meiotic segregation 1 (hPMS1), and NDRG2 are downregulated in ATLL cells through hypermethylation of DNA promoter and is restored by treatment with a DNA demethylation agent, including 5-Azacytidine (5-Aza) [5,14–17]. On the other hand, trimethylation of histone H3 lysine 27 (H3K27me3) mediated by enhancer of zeste homolog 2 (EZH2)-containing polycomb repressive complex 2 (PRC2) contributes to chromatin compaction and recruitment of DNA methyltransferases (DNMTs), leading to the methylation of CpG islands of target genes and induction of the transcriptional silencing of different genes, which may also contribute to cancer development [18,19]. It has been reported that the levels of EZH2 expression and H3K27me3 modification are increased in many types of cancers including ATLL and are associated with tumor progression and poor prognosis, suggesting that trimethylation at H3K27 through overexpression of EZH2 may play an important role in the development and progression of ATLL [20,21]. EZH2 expression is known to be upregulated by bacteria/virus infection [22,23] and signal transduction pathways [24–26], and is also recently reported to be modulated by aberrant signal transduction pathways in HTLV1-induced ATLL tumorigenesis. The pharmacological inhibition or transcriptional silencing of EZH2 result in a decrease in H3K27me3 and restore the expression of tumor suppressor genes in HTLV-1-infected T- and ATLL cells [20], suggesting that promoter methylation and histone modification may play critical roles in the inactivation of tumor suppressor genes, including NDRG2.

In this study, HTLV-1-encoded oncogenic protein Tax was shown to promote NDRG2 expression through Tax-mediated NF-κB activation during early stage of ATLL development. In contrast, sustained Tax expression activated the NF-κB signaling pathway and thereby induced EZH2 expression through the binding of NF-κB to the EZH2 promoter, leading to the suppression of NDRG2 expression via occupancy of EZH2 and H3K27me3 modification on the NDRG2 promoter. Because knockdown of EZH2 through shEZH2 or EZH2 inhibitor revealed a restoration of NDRG2 expression along with suppression of cell proliferation in ATLL cells, the HTLV-1 Tax/NF-κB/EZH2/NDRG2 axis may play an important role in the ATLL leukemogenesis, which may provide a novel approach for the prevention and treatment of ATLL.

2. Materials and methods

2.1. Reagents

The 5-Azacytidine (5-Aza) was obtained from Sigma-Aldrich (St. Louis, MO), and Bay 11-7082 was obtained from Millipore (Temecula, CA). The 3-deazaneplanocin A (DZNep) was obtained from Cayman Chemical (Ann Arbor, MI). The transfection reagents HilyMax and cell proliferation/cell toxicity kit Cell Counting Kit-8 were purchased from DOJINDO (Kumamoto, Japan). Primary antibodies were purchased as indicated: rabbit polyclonal antibodies against IκBα (C-21) and p65 (C20), mouse monoclonal antibody against p100/p52 (C-5), and goat polyclonal antibody against NDRG2 (E20) from Santa Cruz (Santa Cruz, CA), DNMT1 (5032), rabbit polyclonal antibody against EZH2 (4905), rabbit monoclonal antibody against phospho-IKKα/β (Ser176/180) (9554), and mouse monoclonal antibody against phospho-IκBα (Ser32/36) (5A5) from Cell Signaling Technology (Danvers, MA), rabbit polyclonal antibody GFP (598) from MBL (Woburn, MA), rabbit polyclonal antibody against trimethyl-Histone H3 (Lys27) (H3K27me3) from Millipore, and mouse monoclonal antibody against β-actin from Sigma-Aldrich (AC-74, A5316). The mouse monoclonal antibody against Tax (MI73) was a kind gift from Dr. M. Matsuoka (Kyoto University, Japan).

2.2. Plasmid construction

Human EZH2 complementary DNA (cDNA) from MT2 was subcloned into the p3xFLAG-myc-CMV-26 expression vector (Sigma-Aldrich) (Flag-EZH2). The Flag-tagged NDRG2 and p47 expression vector (pCMV26/NDRG2 and pCMV26/p47) has been described elsewhere [5,27]. The small hairpin RNA (shRNA) with the different three oligonucleotides DNA sequences against EZH2 was generated in the RNAi-Ready pSIREN RetroQ-ZsGreen vector (Clontech, Mountain View, CA) (shEZH2#1-3). A control shRNA vector against luciferase was purchased from Clontech (shluc). The NDRG2 promoter region was amplified by PCR and inserted into the pGL4.10 firefly luciferase vector from Promega (Madison, WI). The internal control Renilla luciferase vector pRL-TK was purchased from Promega. To generate the substitution mutant luciferase vector of the NDRG2 promoter, PCR-based mutagenesis was performed to induce the mutation in the NF-κB binding site using mutagenic primers. pCG-Tax is a kind gift from Dr. J. Fujisawa (Kansai Medical University, Japan) [28]. EGFP-p50 and EYFP-p65 were kind gifts from Dr. H. Iha (Oita University, Japan). The transfections were performed using the Amaxa cell line Nucleofector kit V (LONZA, Germany) and HilyMax, following the manufacturer's protocol.

2.3. Cell culture

JPX9 and JPXM are derivatives of the Jurkat T cell line and contain the wild-type or inactive mutant of NF-κB transcriptional activation of the tax gene, respectively, under the control of the inducible metallothionein promoter. Tax expression was induced by the presence of 120 μM Zn^{2+} in the culture medium. Jurkat, MOLT4, and MKB-1 are HTLV-1-negative human T-ALL cell lines. KOB, KK1, and SO4 are IL2–dependent ATLL cell lines. SU9T-01 and ED are IL2-independent ATLL cell lines. MT2 and HUT102 are T-cell lines transfected by HTLV-1 infection. Jurkat, MOLT4 and MKB1 cells were obtained from the Fujisaki Cell Center, Hayashibara Biochemical Laboratories (Okayama, Japan). MT2 and HUT102 cells were a kind gift from Dr. H. Iha (Oita University, Oita, Japan). KOB, KK1, and SO4 cells were kind gifts from Dr. Y. Yamada (Nagasaki University, Japan). SU9T-01 was a kind gift from Dr. N. Arima (Kagoshima University, Japan). ED was a kind gift from Dr. M. Maeda (Kyoto University, Japan). Tax^+ T-cells are HTLV-1 Tax-transformed human peripheral blood mononuclear cells (PBMCs), which were a kind gift from Dr. M Fujii (Niigata University, Japan). Human embryonic kidney 293 T cells were obtained from RIKEN Biorecourse Center (Tsukuba, Japan). IL2-dependent ATLL cell lines were maintained in PRMI1640 medium supplemented with 10% fetal bovine serum (FBS) and 0.75 μg/ml recombinant human IL2 from Peprotech (Rocky Hill, NJ) in a humidified atmosphere of 5% CO_2 at 37 °C. The HTLV-1-negative cell lines and IL2-independent ATLL cell lines were maintained in the same medium without IL2. Other cells were maintained in Dulbecco's Modified Eagle's Medium (DMEM, Wako, Japan) supplemented with 10% FBS.

2.4. Patient samples

Blood samples were obtained from ATLL patients prior to chemotherapy start. This study was performed in accordance with the Declaration of Helsinki and the Japanese Ethical Guidelines for Medical and Health Research Involving Human Subjects and for Human Genomic/Genetic Analysis Research, and approved by the Institutional Review Board of the Faculty of Medicine, University of Miyazaki, Miyazaki, Japan. Informed consent was properly obtained from all participants in this study. The collection of ATLL cells from the patients and $CD4^+$ lymphocytes from volunteers was performed as described previously [29]. Primary leukemic cells from ATLL patients were maintained in AIM-V medium (Thermo Fisher Scientific, Waltham, MA) supplemented with 20% FBS, 10 μM 2-mercaptoethanol (Thermo Fisher Scientific) and 0.75 μg/ml recombinant human IL2 in a humidified atmosphere of 5% CO_2 at 37 °C.

2.5. cDNA synthesis, reverse transcription (RT)-PCR and quantitative real time PCR

Total RNA was isolated from cells using TRIzol reagent (Invitrogen). The cDNA was synthesized from 1 μg of RNA sample with RNA PCR kit with oligo (dT) primer (TaKaRa, Japan) and used as a template for RT-PCR analysis. Quantitative real-time PCR (qPCR) was carried out using Applied Biosystems StepOne Real Time PCR System (Applied Biosystems) and GeneAce SYBR qPCR Mixα (Nippon Gene, Japan). Expression levels of the target gene were normalized to β-actin mRNA.

2.6. Western blotting

For extraction of protein from tissues, excised organs were homogenized in NP-40 lysis buffer (50 mM Tris-HCl, pH 8.0, 150 mM NaCl, 5 mM EDTA, 1% NP-40) supplemented with a proteinase inhibitor cocktail (Sigma-Aldrich) and phosphatase inhibitor tablet (PhosStop, Roche). The lysate was centrifuged for 10 min at 15,000 ×*g* (maximum) at 4 °C, and the supernatant was collected. The protein concentration was determined using the BCA protein assay (Thermo SCIENTIFIC, Waltham, MA) with bovine serum albumin (BSA) standard. Equal amounts of protein samples were loaded, separated by SDS-polyacrylamide gel electrophoresis and then transferred to a polyvinylidene difluoride membrane (PVDF, Immobilon-P, Millipore). The membranes were blocked in PBS-Tween (0.1%) with 1% BSA or 5% nonfat dried milk and then probed with the primary antibodies diluted in PBST-BSA with 5% nonfat dried milk or Can Get Signal Buffer (TOYOBO, Japan). The bands were detected using the Lumi-light Plus kit (Roche) and LAS-3000. Band intensities were quantified with the NIH ImageJ software. All primary antibodies were used at a dilution of 1:1000.

2.7. Chromatin immunoprecipitation (ChIP)-PCR assay

Cells were cross-linked with 1% formaldehyde for 10 min at room temperature. The cells were then washed, lysed, and sonicated to generate 200 to 1000-bp DNA fragments according to BIORUPTOR UCD-250 per the manufacturer's instructions (Cosmo Bio, Tokyo, Japan). The samples were incubated with 1 μg of the indicated antibodies overnight with rotation at 4 °C. Immunoprecipitations were recovered with Protein G Sepharose 4 Fast Flow (GE Healthcare, Uppsala, Sweden), washed, and eluted with elution buffer. Following the reversal of cross-links at 65 °C for 4 h, the samples were extracted with phenol/chloroform, precipitated with ethanol and amplified by PCR. The primers sequences used are listed in Supplemental Table 1.

2.8. Promoter luciferase assay

Cells were transfected with NDRG2 promoter, NF-κB mutant luciferase vector and pRL-TK vector using Amaxa. The transcriptional activity was measured using a dual luciferase assay kit (Promega) according to the manufacturer's instructions with a luminometer (Turner Designs TD-20/20, Promega).

2.9. DNA methylation array

The DNA methylation array analysis using primary ATLL cells has been described in our previous report [5]. Briefly, DNA samples from primary ATLL cells and ATLL-related cell lines were bisulfite-modified using the EZ DNA Methylation-Gold kit (ZYMO RESEARCH, Orange, CA). The bisulfite-treated DNA was analyzed on the Infinium HumanMethylation27 Bead Array (Illumina, San Diego, CA) according to the manufacturer's instructions. The data were analyzed using Genome Studio methylation software (Illumina). Methylation values were calculated as ratio of the methylated/(methylated and unmethylated) fluorescent signals (beta value).

2.10. Bisulfite sequencing

Genomic DNA was treated with bisulfite using the EZ DNA Methylation kit (ZYMO RESEARCH). PCR was performed in a 20-μl volume containing 1 μl of bisulfite-treated DNA, 500 μM of dNTPs and

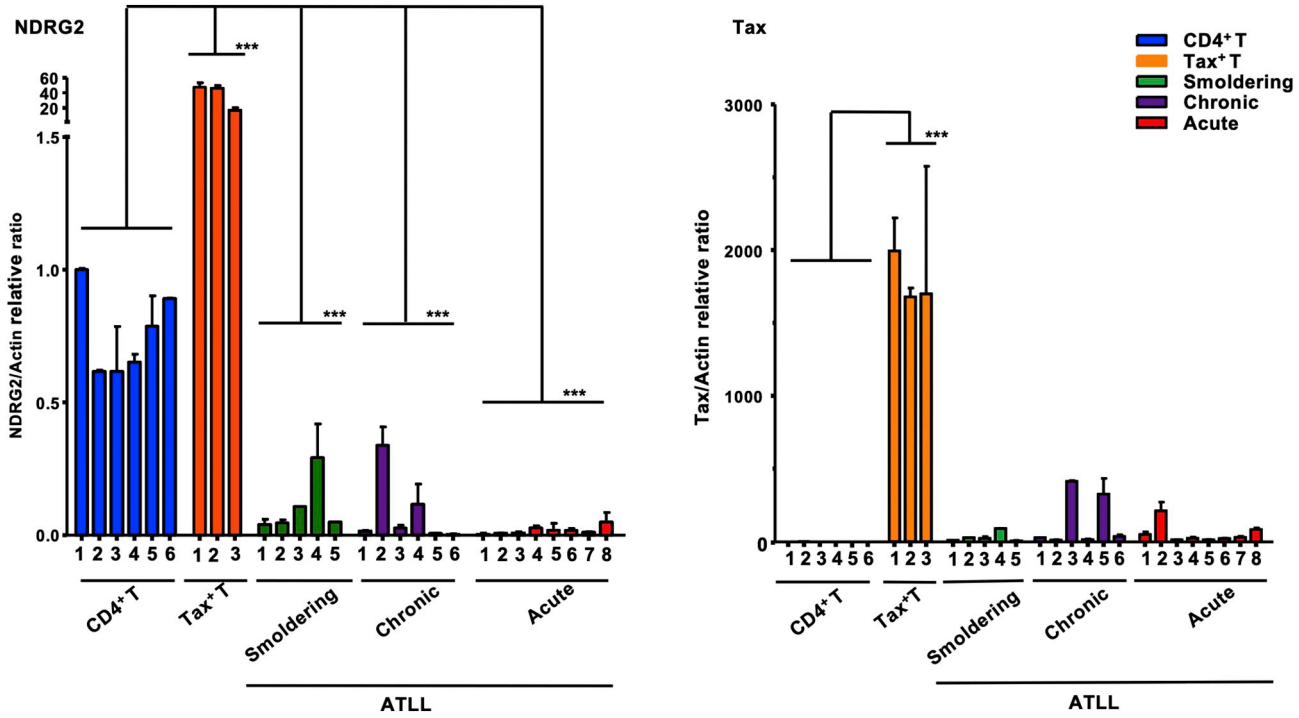

Fig. 1. NDRG2 expression is upregulated in Tax-immortalized T-cells and downregulated in primary ATLL cells, respectively.
Quantitative real-time PCR analysis of NDRG2 and Tax mRNA in $CD4^+$ T-cells from six healthy volunteers ($CD4^+$ T), three Tax-immortalized T-cell lines (Tax^+ T), and leukemic cells from patients with various types of ATLL; five smoldering-types, six chronic-types, and eight acute-types. The data are expressed as the mean and s.d. The Mann-Whitney *U*test was used for statistical analysis (***; $p < 0.01$ compared with $CD4^+$ T cell from the healthy volunteers).

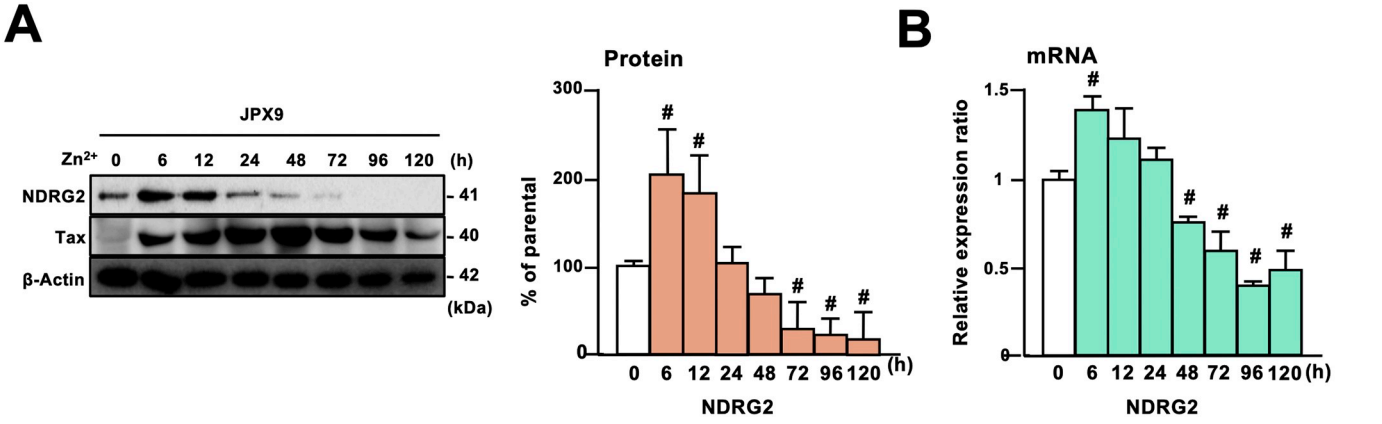

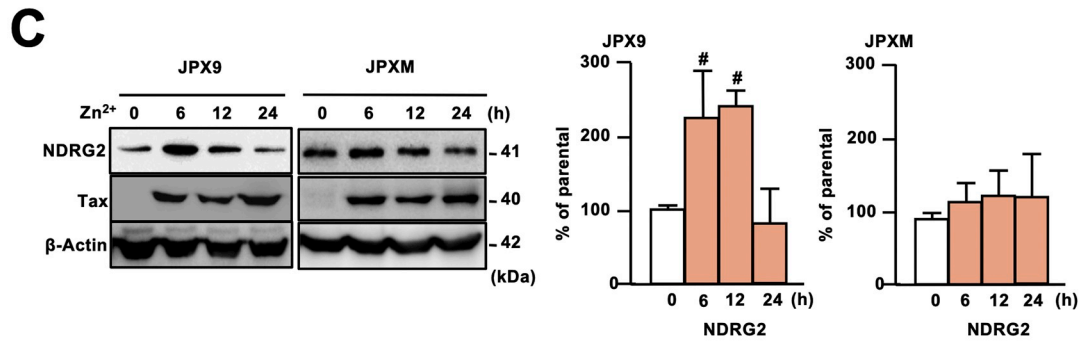

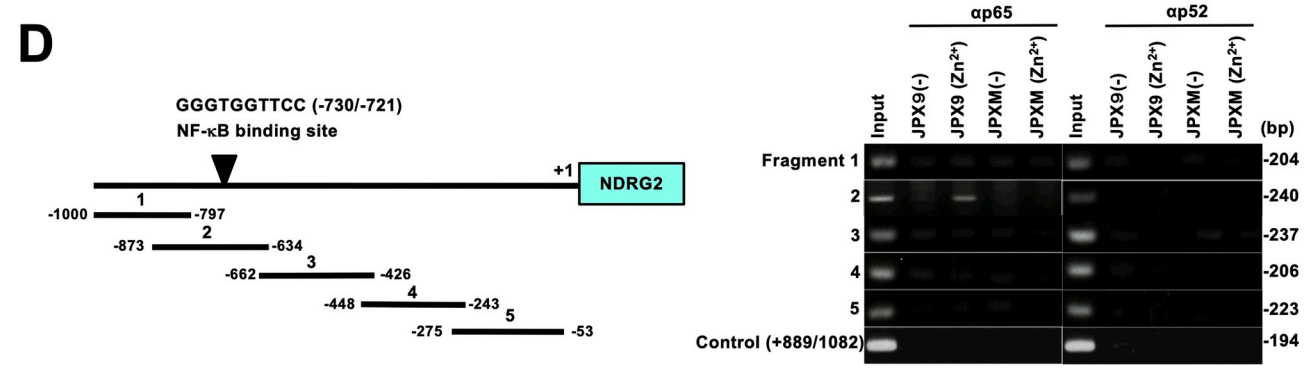

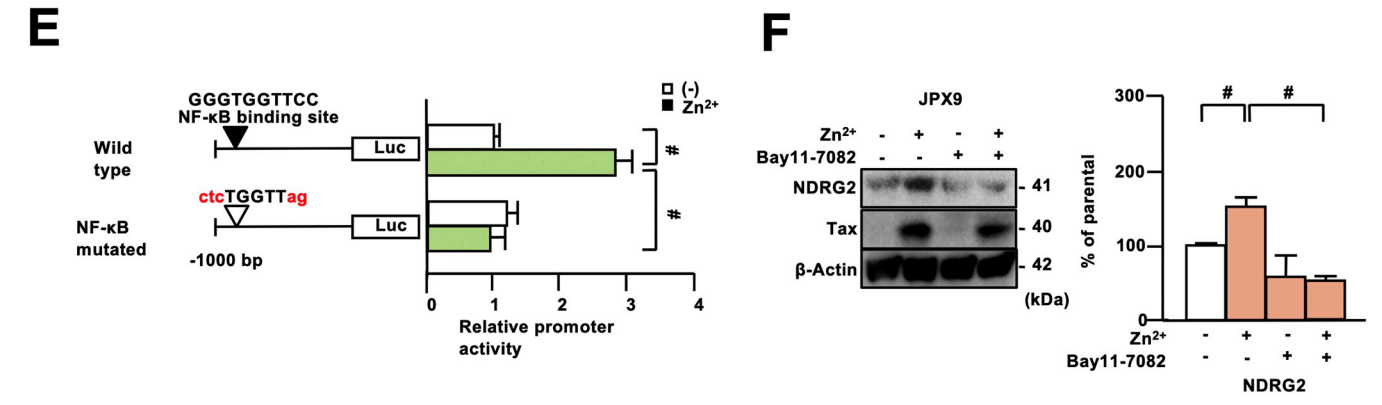

(caption on next page)

Fig. 2. NDRG2 expression is transiently upregulated through the activation of NF-κB after the induction of Tax in T-cell line.
A, JPX9 cells were treated with Zn^{2+} (120 μM) and incubated in RPMI-1640 medium supplemented with 10% FBS for the indicated times, followed by western blot analysis with the indicated antibodies (left panel). The results are representative of three independent experiments. The bar graph shows the quantification of the relative band intensity of NDRG2 normalized by β-actin (right panel). The data are expressed as the mean and s.d. ($n = 3$). Student's *t*-test was used for statistical analysis ($^{\#}$;$p < 0.05$ compared to the untreated control).
B, Quantitative real-time RT-PCR analysis of NDRG2 mRNA in Zn^{2+} (120 μM)-treated JPX9. The data are expressed as the mean and s.d (n = 3). Student's *t*-test was used for statistical analysis ($^{\#}$;$p < 0.05$ compared to the untreated control).
C, Tax-inducible JPX9 or JPXM (loss of NF-κB activation) cell lines were treated with Zn^{2+} (120 μM) and incubated in RPMI-1640 medium supplemented with 10% FBS for the indicated times, followed by western blot analysis with the indicated antibodies. The results are representative of three independent experiments. The graphs show the quantification of the relative band intensity of NDRG2 normalized by β-actin. The data are expressed as the mean and s.d. (n = 3). Student's *t*-test was used for statistical analysis ($^{\#}$;p < 0.05 compared to the untreated control).
D, ChIP-PCR of the NF-κB consensus binding site (−730 to −721 bp) on the human NDRG2 promoter (+1 represents the transcription initiation site) and of a negative control sequence (+889 to +1082 bp) performed using anti-p65 and p52 antibodies in JPX9 and JPXM in the presence or absence of Zn^{2+} (120 μM). The input chromatin (input), which represents a portion of the sonicated chromatin before immunoprecipitation, served as a positive control.
E, JPX9 cells were transfected with a luciferase reporter plasmid with one kb of NDRG2 promoter (−1000 to +1) and pRL-TK plasmid and untreated or treated with Zn^{2+} (120 μM), followed by luciferase reporter assays. For mutation in the NF-κB-binding site (GGGTGGTTCC), five nucleotides (shown in red, ctcTGGTTag) were replaced into the NDRG2 promoter-luciferase reporter vector. The data are expressed as the mean and s.d. ($n = 3$). Student's *t*-test was used for statistical analysis ($^{\#}$;$p < 0.05$).
F, JPX9 cells were treated with or without Zn^{2+} (120 μM) in the presence or absence of Bay11-7082 (10 μM) and incubated in RPMI-1640 medium supplemented with 10% FBS for 6 h, followed by western blot analysis with each indicated antibody. The graph shows the quantification of the relative band intensity of NDRG2 normalized by β-actin. The data are expressed as the mean and s.d. (n = 3). Student's *t*-test was used for statistical analysis ($^{\#}$;p < 0.05).

500 nM of each primer for the NDRG2 promoter region (nucleotides 20564110-20563790, GenBank accession no. NC_000014) (forward 5′-TTTTCGAGGGGTATAAGGAGAGTTTATTTT-3′ and reverse 5′-CCAA AAACTCTAACTCCTAAATAAACA-3′), and 1 unit of Taq polymerase (Takara) under the following conditions: 98 °C for 30 s; 40 cycles of 98 °C for 10 s, 60 °C for 5 s and 72 °C for 30 s; and final extension at 72 °C for 3 min. PCR products were subcloned into the pTA2 vector (TOYOBO) and sequenced.

2.11. Cell proliferation assay

Cells were seeded in 96-well plates at a density of 2×10^3 per well and incubated for the indicated time period in culture medium. Cells were counted using the cell counting kit-8.

2.12. Statistical analysis

Data are presented as the means and s.d. We used the two-tailed Student's *t*-test and Mann-Whitney *U*test for comparisons within each parameter. A probability value $p < 0.05$ was considered statistically significant.

3. Results

3.1. NDRG2 expression is upregulated and downregulated in Tax-immortalized T-cells and primary ATLL cells, respectively

We previously reported that NDRG2 expression is downregulated in ATLL cells by genomic deletion and DNA methylation of the NDRG2 promoter [5]. To elucidate detailed mechanisms of NDRG2 downregulation during ATLL leukemogenesis, we initially determined the expression levels of NDRG2 and HTLV-1/Tax in peripheral $CD4^+$ T-cells from healthy volunteers, Tax-immortalized T-cells (Tax^+ T), and leukemia cells from patients with smoldering-type, chronic-type, or acute-type ATLL (Fig. 1). Surprisingly, the expression of NDRG2 was significantly upregulated in Tax^+ T-cells compared with $CD4^+$ T-cells from healthy volunteers, suggesting that HTLV-1/Tax may enhance NDRG2 expression. In contrast, the NDRG2 expression was downregulated in primary ATLL cells from patients with various types of ATLL and it was gradually decreased during stage progression of ATLL. Although Tax mRNA was highly expressed in Tax-immortalized T-cells, moderately or low level of the Tax expression was detected in primary leukemic cells from various types of ATLL cases as reported previously [5].

3.2. Tax expression transiently activates the NDRG2 promoter through the NF-κB pathway in Tax-inducible JPX9 cell line

Because the NDRG2 expression is induced by various cellular stress responses such as inflammation, hypoxia, and oxidative stress [6–11], the HTLV1 infection may induce NDRG2 expression. To determine whether HTLV-1/Tax induces NDRG2 expression, we utilized a Tax-inducible JPX9 cell line, which is a derivative of Jurkat/T-ALL cell line containing the Tax gene under the control of Zn^{2+}-inducible metallothionein promoter. The protein and mRNA expression levels of NDRG2 were mildly increased along with induction of the Tax expression at 6 to 12 h after the Zn^{2+} treatment, and then gradually decreased to the expression level of NDRG2 less than the basal level in the untreated JPX9 cell line at 72 h (3 days) to 120 h (5 days) during the induction of Tax expression (Fig. 2A, B, and Supplementary Fig. 1A). To determine whether the observed transient induction of NDRG2 by the Tax expression was mediated by the NF-κB pathway, one of the most important pathways activated by Tax, we used the JPXM cell line containing a Tax mutant that is defective in inducing NF-κB activation and control JPX9 cell line to measure NDRG2 induction at 6 to 24 h after Zn^{2+} treatment. In JPX9 cells, NDRG2 expression increased after 6 h of treatment then decreased at 24 h; however, NDRG2 expression in the JPXM cell line did not change at any time point after Zn^{2+} treatment with mutated Tax induction (Fig. 2C). In JPX9 cells treated with Zn^{2+}, the canonical NF-κB pathway was activated with increased levels of phosphorylated IKK-Ser176/180 and IκBα-Ser32/36 proteins and reduced protein level of IκBα (Supplementary Fig. 1B). The non-canonical NF-κB pathway was also activated with p100 processing to p52. However, neither the canonical nor non-canonical NF-κB pathways were activated by the induction of mutated Tax in the JPXM cells (Supplementary Fig. 1B). Since transfection of the expression vectors for the canonical NF-κB p65 and p50 into 293T cells induced NDRG2 expression, the activation of NF-κB signaling pathway is necessary for induction of NDRG2 (Supplementary Fig. 1C).

To assess whether the NF-κB transcription factors directly bind and activate the NDRG2 promoter following the Tax induction, we performed chromatin immunoprecipitation (ChIP) assays using antibodies against p65 or p52 in the JPX9 cell line. Based on an analysis of the genomic sequence of the human NDRG2 promoter within −1000 bp upstream of the transcriptional start site, an NF-κB consensus sequence was found in the region from nucleotides of −730 to −721 (Fig. 2D). Cell extracts from JPX9 or JPXM cell lines with or without Zn treatment were immunoprecipitated using an anti-p65 antibody for the canonical NF-κB pathway or anti-p52 antibody for the non-canonical pathway and then amplified by each specific primer pair to recover five DNA

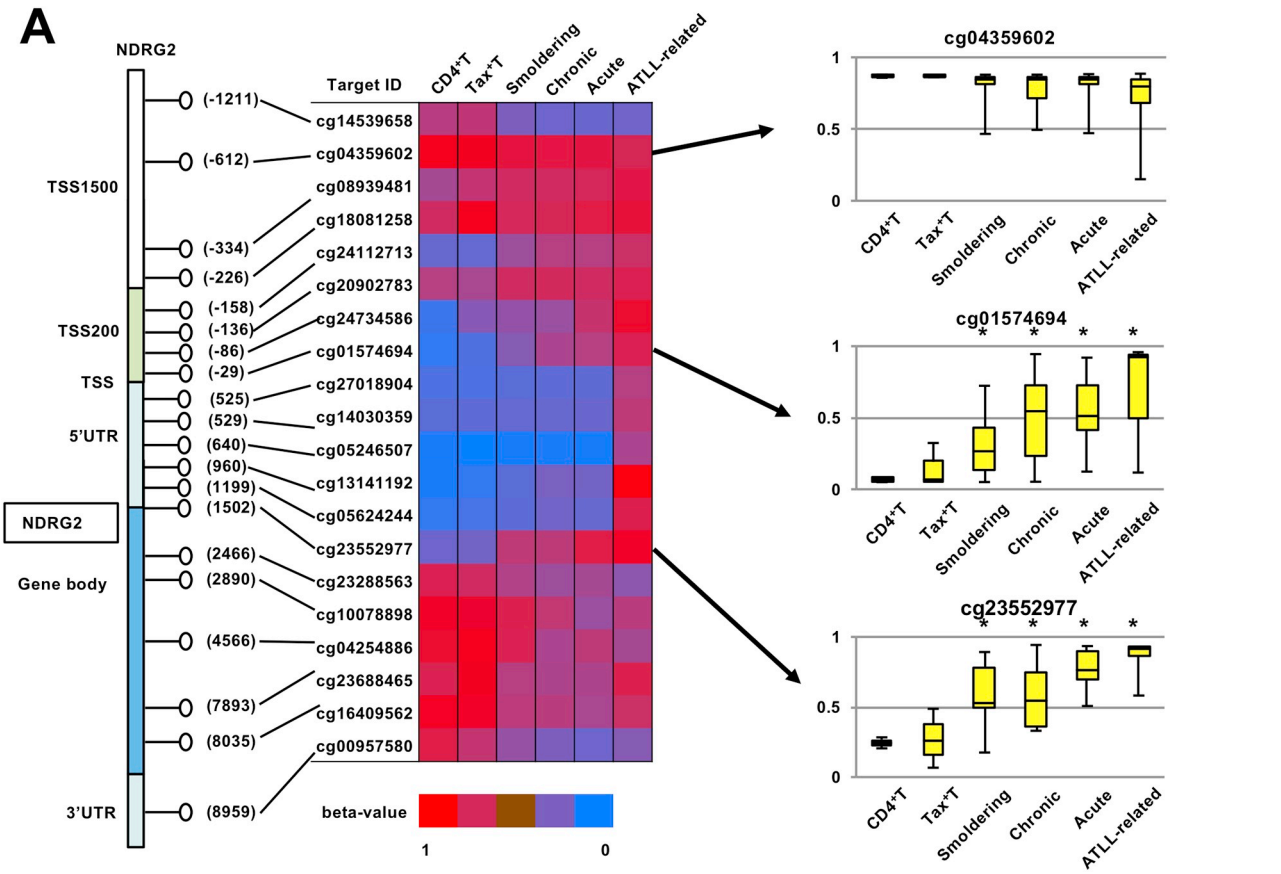

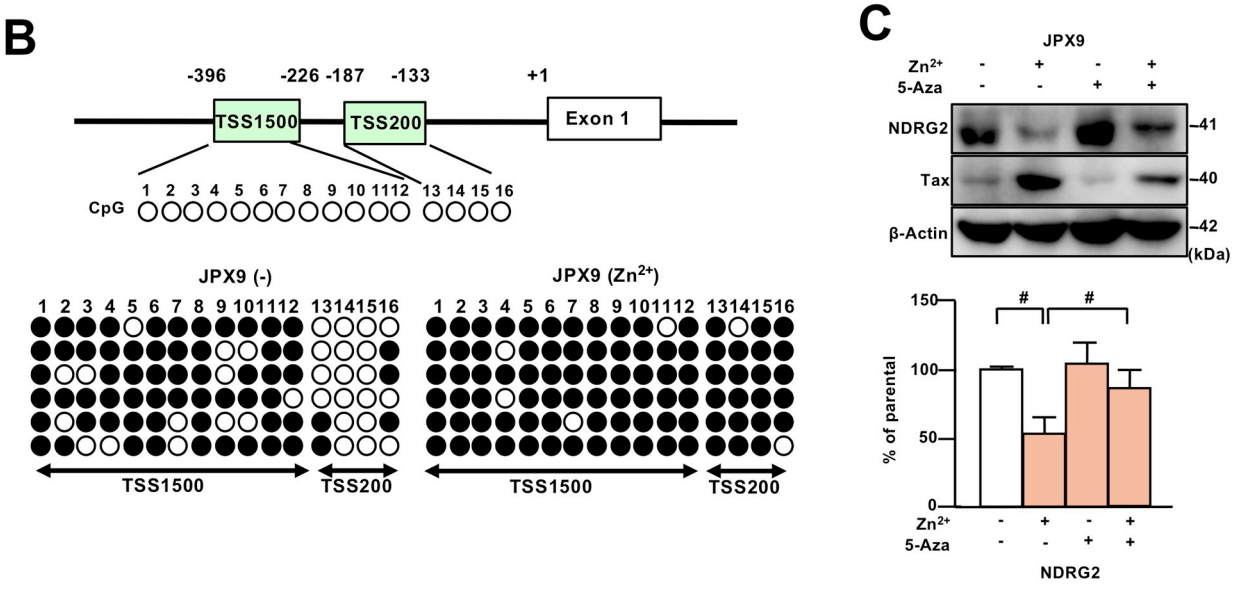

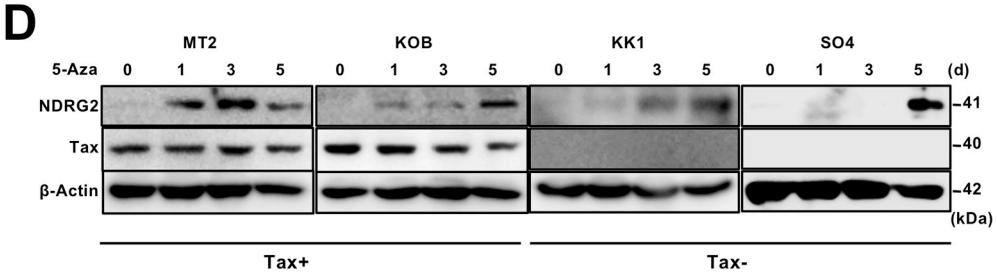

(caption on next page)

Fig. 3. Downregulation of NDRG2 expression through DNA promoter methylation.
A, A heat map showing the levels of DNA methylation in the CpG islands in the NDRG2 gene. TSS200 and TSS1500 represent 1–200 bp and 200 to 1500 bp upstream from the TSS (translation start site), respectively. UTR, untranslated region; gene body, exon and intron. DNA methylation levels were shown as the average beta value, which is represented by the scale with the highest methylation value (1) in red and the lowest (0) in blue. DNA samples from $CD4^+$ T-cells from five healthy volunteers [$CD4^+$T], three Tax-immortalized cell lines [Tax^+T], leukemic cells from patients with ten smoldering-types, eleven chronic-types, and nine acute-types were analyzed. Box plot with median (horizontal line inside the box), lower (25%) and upper (75%) quartile (box limits), and the lowest and highest scores (whiskers) is also shown on the right. Student's *t*-test was used for statistical analysis (*;$p < 0.05$ compared with the healthy controls).
B, CpG island region in the NDRG2 promoter was amplified by PCR using bisulfite-treated genomic DNA of JPX9 cells treated with or without Zn^{2+} (120 μM) for three days and the PCR products were subcloned, followed by sequencing analysis. Open circles indicate unmethylated CpGs, and filled circles indicate methylated CpGs.
C, JPX9 cells were pretreated with or without Zn^{2+} (120 μM) in the presence or absence of 5-Aza (5 μM) and incubated in RPMI-1640 medium supplemented with 10% FBS for three days, followed by western blot analysis with the indicated antibodies. The graph shows the quantification of the relative band intensity of NDRG2 normalized by β-actin. The data are expressed as the mean and s.d. ($n = 3$). Student's *t*-test was used for statistical analysis ($^\#$;$p < 0.05$).
D, MT2, KOB, KK1, and SO4 (ATLL-related cell lines) were treated with 5-Aza (5 μM) for one to five days and subjected to western blot analysis with the indicated antibodies.

fragments (No. 1 to No. 5) covering the 1.0-kb promoter region. A DNA of the fragment 2 (nucleotides of −873 to −634) containing the NF-κB-binding site (−730 to −721) was amplified from cell extracts of JPX9 by anti-p65 antibody, but not from those of JPXM after the treatment with Zn^{2+}; however, none of the DNA fragments were co-immunoprecipitated by the anti-p52 antibody (Fig. 2D), suggesting that the canonical NF-κB pathway was activated in JPX9 cells. To confirm whether the expression of NDRG2 was mediated by the activation of NF-κB signaling pathway, a luciferase reporter vector containing the 1.0-kb NDRG2 promoter region was generated and transfected into JPX9 cells, and the promoter activity of the 1.0-kb fragment was determined. After Zn^{2+} treatment to the transfected JPX9 cells, the promoter activity of the 1.0-kb fragment of NDRG2 promoter was increased up to 3-fold as compared to that of untreated cells, and the activity of the promoter was abrogated in the luciferase construct with mutated NF-κB consensus sequence (Fig. 2E). To further confirm the NF-κB-dependent transcriptional activation of NDRG2, an NF-κB inhibitor, Bay11-7082, was applied in the JPX9 inducible system. The treatment of Bay11-7082 significantly inhibited Tax-induced NDRG2 expression after the Zn^{2+} treatment (Fig. 2F), suggesting that activation of the NF-κB pathway is important for the activation of NDRG2 expression during early phase of Tax induction.

3.3. Downregulation of NDRG2 expression by DNA promoter methylation

To determine the levels of DNA methylation of the NDRG2 promoter during ATLL leukemogenesis, we performed a DNA methylation array analysis with genomic DNA from $CD4^+$ T-cells from healthy volunteers, Tax^+ T-cells, and leukemia cells from patients with various types of ATLL [5]. The region between −158 from the transcription start site (TSS) to 1502 in the 5′ untranslated region (5′UTR) of the NDRG2 gene was unmethylated in $CD4^+$ T-cells; however, the levels of DNA methylation in the promoter region (TSS200) from −158 to −29 were gradually increased during ATLL progression from Tax^+ T, smoldering-, chronic- to acute-type ATLL cells (Fig. 3A and Supplementary Fig. 2A).

To next determine whether the Tax expression affects the methylation status of the NDRG2 promoter region, JPX9 cells treated with Zn^{2+} were subjected to bisulfite sequencing. The upstream CpG island (CpG 1 to 12) from −396 to −226 in TSS1,500 was highly methylated, which is probably due to the fact that the JPX9 cell line was established 30 years ago; however, the downstream CpG islands (CpG 13 to 16) from −187 to −133 in TSS200 was clearly unmethylated. After induction of Tax protein by Zn^{2+} for three days, those CpGs (13 to 16) were heavily methylated (Fig. 3B), suggesting that the Tax expression may promote the DNA methylation in the NDRG2 promoter region.

To determine whether DNA methylation at the CpGs (13 to 16) induced by the Tax expression affects NDRG2 expression, Tax-inducible JPX9 cells were co-treated with 5-azacytidine (5-Aza), an inhibitor of DNA methylation during the Zn^{2+} treatment. After 5-Aza treatment of JPX9 with or without Zn^{2+} for three days, the NDRG2 expression was restored by the treatment of both 5-Aza and Zn^{2+}, while Zn^{2+} single treatment suppressed expression of NDRG2 (Fig. 3C). The similar results were obtained in the treatment with 5-Aza to Tax-transfected 293T cell line (Supplementary Fig. 2B and C). Moreover, we determined whether 5-Aza treatment restores the expression of NDRG2 in four ATLL-related cell lines (Tax-positive MT2 and KOB, Tax-negative KK1 and SO4), which had highly methylated NDRG2 promoter in TSS200 (Supplementary Fig. 2D and E). The 5-Aza treatment restored NDRG2 expression in all of the four ATLL-related cell lines (Fig. 3D and Supplementary Fig. 2F). Therefore, DNA methylation of the NDRG2 promoter plays an important role in the suppression of NDRG2 expression in both HTLV1-infected and ATLL cells via Tax-dependent and -independent mechanisms.

3.4. Suppression of NDRG2 expression by the polycomb group protein EZH2-mediated epigenetic modifications

To identify the proteins that regulate the DNA methylation of the NDRG2 promoter, we analyzed gene expression prolife of ATLL patient samples using the DNA microarray [5] and particularly determined a series of enzymes and transcription factors related to DNA methylation. We observed a significant upregulation of enhancer of zeste homolog 2 (EZH2), one of the components of the polycomb repressive complex (PRC2), in ATLL compared with control $CD4^+$ T-cells. However, the expression level of DNA methyltransferase (DNMT) family did not change (Supplementary Fig. 3A). Since PRC2 has been reported to play an important role in regulation of the expression of tumor suppressor genes through trimethylation of Lys27 in histone H3 (H3K27me3) in HTLV-1-infected and ATLL cells [20], we analyzed the expression of EZH2 and H3K27me3 in primary ATLL cells and ATLL cell lines. The mRNA and protein levels of EZH2 with H3K27me3 modification were significantly increased in primary ATLL cells and ATLL cell lines compared with those in $CD4^+$ T-cells from healthy volunteers and T-ALL cell lines, respectively (Fig. 4A, B and supplementary Fig. 3B). To determine whether Tax induces the expression of DNA methylation factors, we examined the levels of EZH2 expression with H3K27me3 modification and DNMT1 in the Tax-inducible JPX9 cells with or without Tax induction. While the induction of Tax by the Zn^{2+} treatment increased NDRG2 expression through the activation of NF-κB signaling pathway within 6 h (Fig. 2A and B), the protein level of EZH2 and the methylation level of H3K27me3 gradually increased at 12 h to 96 h (four days) after Tax induction, resulting in the inversely reduced NDRG2 protein at 12 h after Tax induction (Fig. 4C, D, and Supplementary Fig. 3C to 3E). Since one of the functions of PRC2 complex with EZH2 recruits DNMT to enhance DNA methylation [18,19], enhanced expression of EZH2 by Tax may play a critical role in the downregulation of NDRG2 expression by promoter methylation.

To confirm whether EZH2 is primarily responsible for the suppression of NDRG2 expression in JPX9 cells, 3-deazaneplanocin A (DZNep), an EZH2 inhibitor, was administered to the JPX9 cells with or without

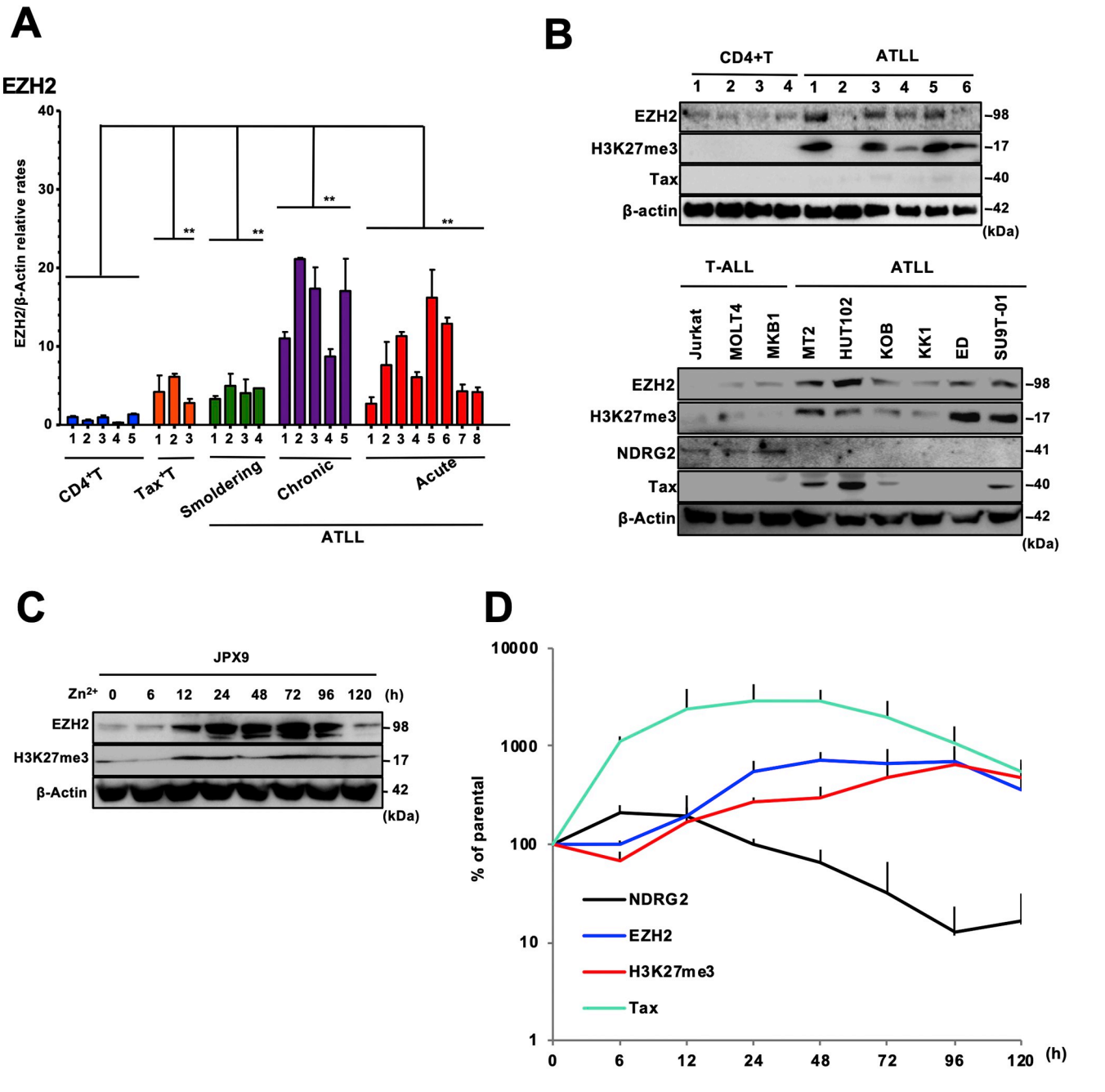

(caption on next page)

Fig. 4. Suppression of NDRG2 expression by polycomb EZH2-mediated epigenetic modification.
A, Quantitative real-time RT-PCR analysis of EZH2 in $CD4^+$T cells from five healthy volunteers ($CD4^+$T), three Tax-immortalized T-cell lines (Tax^+T), and leukemic cells from patients with various types of ATLL; four smoldering-types, five chronic-types, and eight acute-types. The data are expressed as the mean and s.d. The Mann-Whitney *U*test was used for statistical analysis (**;$p < 0.01$ compared with the healthy controls).
B, Expression of EZH2, H3K27me3, and Tax were determined in $CD4^+$ T-cells from four healthy volunteers, leukemic cells from six ATLL patients with acute-type (upper panel), and three T-ALL cell lines as control non-HTLV-1 infection and six ATLL-related cell lines (lower panel) by immunoblot analysis.
C, JPX9 cells were treated with Zn^{2+} (120 μM) and incubated in RPMI-1640 medium supplemented with 10% FBS for each indicated time period (hour), followed by western blot analysis with each indicated antibody. The results are representative of three independent experiments.
D, The graphs show the quantification of the relative band intensity of NDRG2, EZH2, H3K27me3 and Tax normalized by β-actin. The data are expressed as the mean and s.d. (n = 3). Student's *t*-test was used for statistical analysis ($^{\#}$;$p < 0.05$ compared to the untreated control).
E, JPX9 cells were pretreated with or without Zn^{2+} (120 μM) in the presence or absence of DZNep (1 μM) and incubated in RPMI-1640 medium supplemented with 10% FBS for three days, followed by western blot analysis with each indicated antibody (left panel). The graphs show the quantification of the relative band intensity of NDRG2, EZH2, and H3K27me3 normalized by β-actin (three right panels). The data are expressed as the mean and s.d. ($n = 3$). Student's *t*-test was used for statistical analysis ($^{\#}$;$p < 0.05$).
F, MT2, KOB, KK1, and SO4 in ATLL-related cell lines were treated with DZNep (1 μM) for one to five days and subjected to western blot analysis with the indicated antibodies.
G, Cell growth curves of four ATLL-related cell lines (MT2, KOB, KK1, and SO4) were shown under the culture with various doses of DZNep (0 to 1 μM) at each different time period, as assessed using the cell counting kit-8. The data are expressed as the mean and s.d. ($n = 3$). Student's *t*-test was used for statistical analysis ($^{\#}$;$p < 0.05$ compared to the untreated control).
H, Four ATLL-related cell lines (MT2, KOB, KK1, and SO4) were transiently transfected with three shRNA expression vectors targeting with each different targeted region of EZH2 or for control mock luciferase vector (shLuc), followed by western blot analysis for EZH2, H3K27me3, and NDRG2.
I, Two primary leukemia cells from the patients with ATLL cells were treated with DZNep (1 μM) for one to five days and subjected to western blot analysis with the indicated antibodies.
J, Two cases of primary ATLL cells under culturing with various doses of DZNep (0–1 μM) were counted their viable cells at different time periods, by the cell counting kit-8. Student's *t*-test was used for statistical analysis ($^{\#}$; $p < 0.05$ compared to the untreated control).

Zn^{2+} treatment for three days. The NDRG2 expression was suppressed by Zn^{2+} treatment, which was accompanied by upregulation of EZH2 and enhanced H3K27 trimethylation; however, DZNep treatment with Zn^{2+} suppressed the EZH2 expression and the H3K27 trimethylation, resulting in restored expression of NDRG2 (Fig. 4E). Furthermore, when DZNep was administered to two Tax-high (MT2 and KOB) and two Tax-low expressed (KK1 and SO4) ATLL-related cell lines, EZH2 expression as well as H3K27 trimethylation gradually decreased over time after treatment with DZNep, which inversely induced the NDRG2 expression (Fig. 4F and supplementary Fig. 3F). Furthermore, the DZNep treatment suppressed the cell growth rate of ATLL-related cell lines in a dose-dependent manner (Fig. 4G). Additionally, transfection of small hairpin RNA (shRNA)-expression vector targeting EZH2 induced demethylation at H3K27, resulting in the induction of NDRG2 expression in HTLV-1-infected and ATLL cell lines (Fig. 4H). Finally, we determined the effects of DZNep treatment on NDRG2 expression and cell proliferation using primary leukemic cells from ATLL patients. The DZNep treatment of primary ATLL cells suppressed the EZH2 expression and H3K27 trimethylation, and cell proliferation, and upregulated the NDRG2 expression with time-dependent manner (Fig. 4I, J and Supplementary Fig. 3G), indicating that EZH2 overexpression is a major cause of the downregulation of NDRG2 expression in ATLL.

3.5. Direct binding of EZH2 on the NDRG2 promoter to suppress the NDRG2 expression

EZH2-induced H3K27 methylation and the direct binding of EZH2 to target promoter are associated with heterochromatin formation, resulting in DNA promoter methylation to induce transcriptional repression [30,31]. Given that overexpression of EZH2 in 293T cells induced H3K27 trimethylation with dose-dependent suppression of NDRG2 expression and the NDRG2 promoter activity (Supplementary Fig. 4A and B), we next analyzed the direct DNA binding of EZH2 and H3K27me3 modification on the NDRG2 promoter using ChIP-PCR assays with anti-Flag or anti-H3K27me3 antibodies. When five DNA fragments encompassing the 1.0-kb NDRG2 promoter region were amplified after transfection of Flag-tagged EZH2 to 293T cells and immunoprecipitation of sheared DNA with each specific antibody, the DNA fragment 5 (nucleotide −275 to −53) in the CpG island region of the NDRG2 promoter was co-immunoprecipitated with EZH2 or K27 trimethylated histone H3 (Fig. 5A), indicating the binding of EZH2 to the fragment 5 containing with CpG No. 13 to 16 in TSS200 of the NDRG2 promoter with H3K27 trimethylation. Furthermore, after DZNep treatment of ATLL-related cell lines, the binding of DNA fragment 5 to EZH2 and K27 trimethylated Histone H3 was decreased along with demethylation of CpG (13 to 16) in the NDRG2 promoter region (TSS200) (Fig. 5B and C), suggesting that overexpression of EZH2 in HTLV-1-infected and ATLL cells contributes to the suppression of NDRG2 expression via both histone modification and DNA promoter methylation.

3.6. Upregulation of EZH2 expression through the NF-κB pathway in ATLL cells

Because EZH2 expression is regulated by virus and stress-induced NF-κB pathway in many types of cancer [22,23], we assessed whether the activation of NF-κB pathway is involved in EZH2 overexpression in HTLV-1-infected and ATLL cells. After Tax induction in JPX9 cells treated with Zn^{2+} for three days, the levels of EZH2 expression and H3K27 trimethylation were significantly increased, along with inverse reduction of NDRG2 expression; however, the levels of EZH2, H3K27me3, and NDRG2 did not change after the induction of a mutated Tax protein, which is unable to induce NF-κB activation, in JPXM cells (Fig. 6A). In addition, transfection of NF-κB transcription factor, p50 and/or p65 or of Tax expression plasmid, enhanced the EZH2 expression in 293T cells (Supplementary Fig. 5A and B). Furthermore, the treatment of NF-κB inhibitor Bay11-7082 suppressed EZH2 expression in JPX9 with Tax induction after Zn^{2+} treatment, which was accompanied by the suppression of H3K27 trimethylation and downregulation of NF-κB signaling pathway in HTLV-1-infected and ATLL cell lines with Tax (MT2 and KOB) or without Tax expression (KK1 and SO4) (Fig. 6B, C and Supplementary Fig. 5C). The suppression of NF-κB signaling pathway by Bay11-7082 in ATLL cell lines resulted in impaired binding of EZH2 to the NF-κB element in the fragment 5 on the NDRG2 promoter with demethylation of H3K27 (Fig. 6D).

Among many genetic and epigenetic abnormalities involved in Tax-independent NF-κB activation in ATLL cells, we recently found that downregulation of tumor suppressor NDRG2 in ATLL cells activates canonical NF-κB signaling pathway via the activation of PI3K/AKT signaling pathway, and that protein degradation of p47, a negative regulator of NF-κB pathway acting by inducing lysosomal degradation of polyubiquitinated NEMO, also activates canonical NF-κB pathway [4,27]. When NDRG2 or p47 was enforcedly expressed in Tax-negative

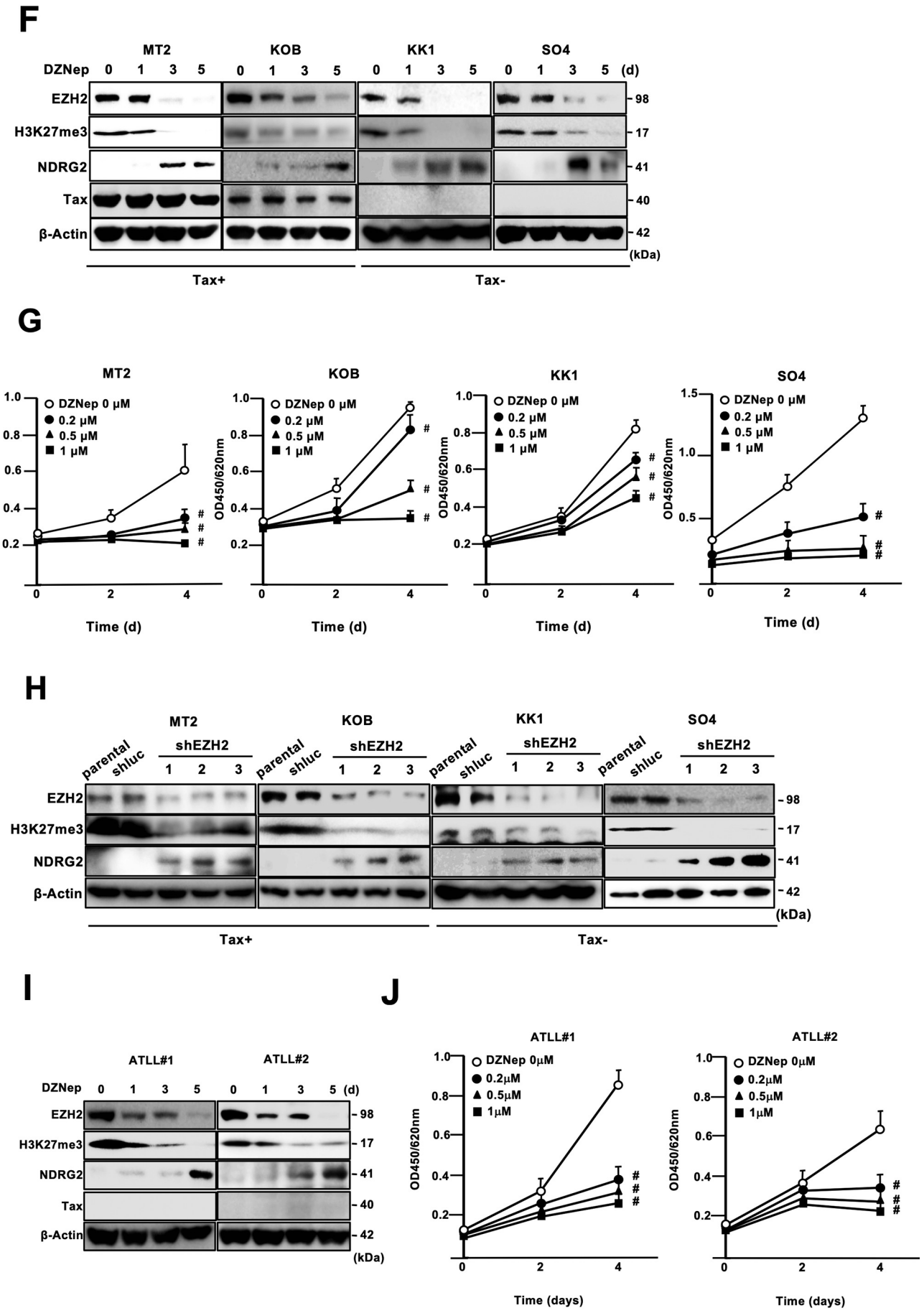

Fig. 4. (*continued*)

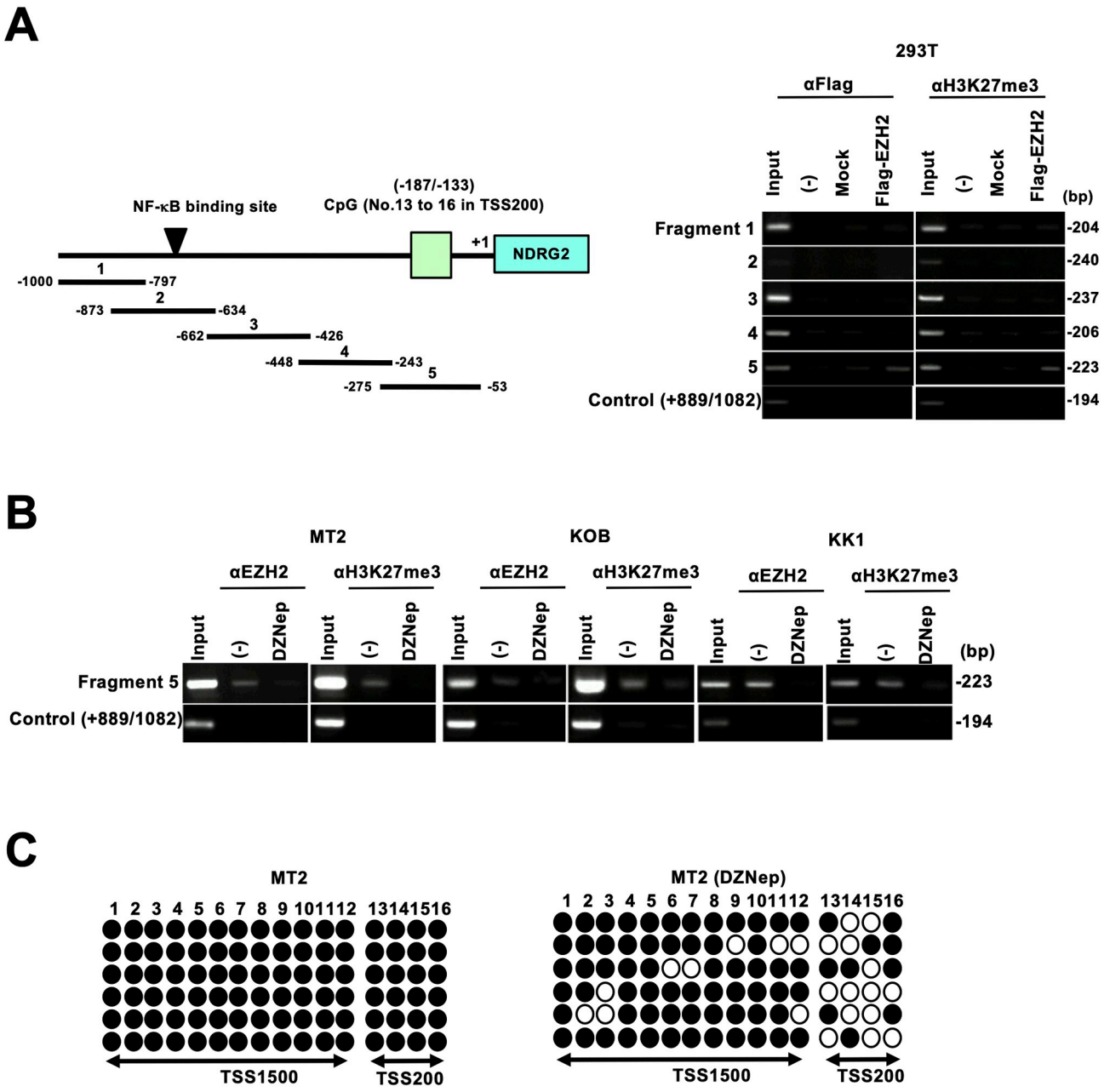

Fig. 5. Direct binding of EZH2 on the NDRG2 promoter.

A, (left panel) The map of the NDRG2 promoter from −1000 to +1 (TSS) is shown with NF-κB binding site (−730 to −721) and CpG island (−187 to −133). Five fragments (No. 1 to No. 5) are indicated their location as amplified DNA fragments by PCR after chromatin immunoprecipitation.

(Right panel) After transfection with Flag-tagged EZH2 in 293T cells, ChIP-PCR was performed by each specific primer for five DNA fragments (No.1 to 5) indicated in left panel, after immunoprecipitation by anti-Flag or antiH3Me27m3 antibody.

B, The same ChIP-PCR as Fig. 5A were performed at the No 5 fragment of NDRG2 promoter in MT2, KOB, and KK1 cell lines with or without the DZNep treatment (1 μM).

C, After the treatment of DZNep (1 μM) to MT2 cells, two CpG regions in the NDRG2 promoter at TSS1500 and TSS200 were amplified by PCR using bisulfite-treated genomic DNA and were sequenced. Open circles indicate unmethylated CpGs, and filled circles indicate methylated CpGs.

and positive ATLL cells, EZH2 expression and the levels of H3K27 trimethylation were significantly decreased by the expression of NDRG2 or p47 through the inhibition of canonical NF-κB signaling pathway (Fig. 6E, F and Supplementary Figs. 5D, E).

NF-κB consensus sequences are found within 696 bp upstream of the TSS in the EZH2 promoter region, and the NF-κB-binding site between −180 bp and −171 bp has been shown to be associated with EZH2 overexpression in ATLL [20,32]. The occupancy of p65 at the NF-κB-binding site in the EZH2 promoter region was clearly detected in JPX9 cells expressing Tax, but not in JPXM cells expressing a Tax mutant (Supplementary Fig. 5F). Furthermore, the treatment of NF-κB inhibitor Bay11-7082 in HTLV-1-infected (MT2) and ATLL (KK1) cell lines suppressed the binding of p65 to the NF-κB-binding site in EZH2 promoter (Supplementary Fig. 5F), indicating that NF-κB activation increases EZH2 expression by promoting the occupancy of NF-κB transcriptional factor p65 on the EZH2 promoter and thereby induces the suppression of NDRG2 expression.

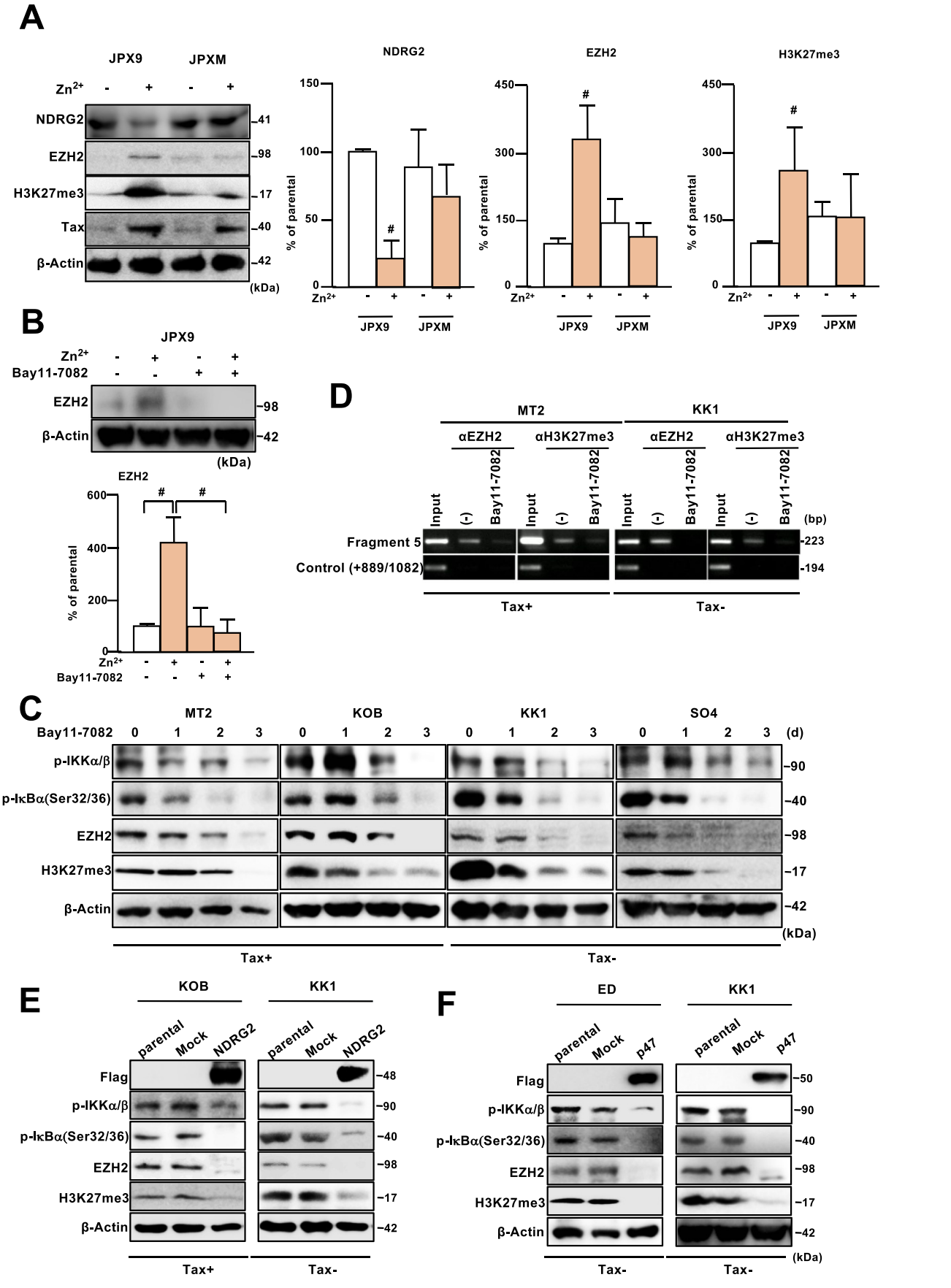

(caption on next page)

Fig. 6. Upregulation of EZH2 expression through the NF-κB pathway.
A, JPX9 and JPXM cells were treated with Zn^{2+} (120 μM) and incubated in RPMI-1640 medium supplemented with 10% FBS for three days, followed by western blot analysis with the indicated antibodies (left panel). The results are representative of three independent experiments. The graphs show the quantification of the relative band intensity of NDRG2, EZH2 and H3K27me3 normalized by β-actin (three right panels). The data are expressed as the mean and s.d. (n = 3). Student's *t*-test was used for statistical analysis ($^{\#}$;$p < 0.05$ compared to the untreated control).
B, JPX9 cells were treated with or without Zn^{2+} (120 μM) in the presence or absence of Bay11-7082 (10 μM) and incubated in RPMI-1640 medium supplemented with 10% FBS for three days, followed by western blot analysis with the indicated antibodies (left panel). The graph shows the quantification of the relative band intensity of EZH2 normalized by β-actin (right panel). The data are expressed as the mean and s.d. (n = 3). Student's *t*-test was used for statistical analysis ($^{\#}$;$p < 0.05$).
C, Four different ATLL-related cell lines (MT2, KOB, KK1, and SO4) were treated with Bay11-7082 (10 μM) for three days and subjected to western blot analysis with each indicated antibody and at each indicated period. Activation of NF-κB is indicated by the level of phosphorylated IKKα/β and phosphorylated IκBα.
D, ChIP-PCR of fragment No. 5 on the human NDRG2 promoter was performed after immunoprecipitation by anti-EZH2 or H3K27me3 antibody in MT2, and KK1 cells with or without Bay11-7082 (10 μM) treatment.
E, KOB, and KK1 cells were stably transfected with the Flag-tagged NDRG2 expression vector (pCMV26/NDRG2), followed by western blot analysis for EZH2 and H3K27me3.
F, ED, and KK1 cells were transiently transfected with the Flag-tagged p47 expression vector (pCMV26/p47), followed by western blot analysis for EZH2 and H3K27me3.

4. Discussion

In this study, to determine how NDRG2 expression is regulated in HTLV-1 infection and in ATLL cells, we determined the NDRG2 expression in various types of Tax-immortalized T-cells, HTLV-1 infected and ATLL cell lines and primary ATLL cells. We showed that NDRG2 expression is upregulated in Tax-immortalized T-cells by Tax-mediated NF-κB activation; however, Tax expression downregulates the NDRG2 expression by enhancing EZH2 expression after the long incubation period in HTLV-1-infected T-cell lines, ATLL cell lines and primary ATLL leukemia cells. Moreover, EZH2 directly occupied the CpGs of NDRG2 promoter with enhanced its DNA methylation and histone methylation at H3K27me3 in HTLV-1-infected and ATLL cells (Supplementary Fig. 6). Thus, although NDRG2 expression may suppress the activation of stress-induced aberrant signaling pathways, chronic stress responses such as virus infection and inflammation may suppress NDRG2 expression via epigenetic modifications by enhanced EZH2 expression through activated NF-κB signaling pathway, which may contribute to tumor development through continuous chronic inflammation responses.

NDRG2 expression is upregulated by several stress responses, including DNA damage by p53, hypoxia by HIF1α, oxidative stress, inflammation [6–11], steroid, and hormones [33,34], implicating a role of NDRG2 in stress-related physiological and pathological processes. Moreover, in Sertoli cell syndrome or hypospermatogenesis, NDRG2 expression is upregulated by testicular Leydig cell-specific toxicant ethane-dimethanesulfonate (EDS) or TNFα through NF-κB-mediated transcriptional activation of the *Ndrg2* promoter, resulting in induction of apoptosis of Leydig cells and male fertility. This apoptosis induction by NDRG2 may play an important role in defense by eliminating damaged sperm cells [11]. Our results also suggest that NDRG2 upregulation following Tax induction may work to avoid excessive proliferative stimulation in HTLV-1-infected T-cells.

NDRG2 expression is significantly downregulated in many types of cancer through DNA promoter methylation and the upregulation of microRNAs, contributing to poor prognosis and survival [35–38]. We showed that the NDRG2 expression was downregulated by the conversely enhanced NDRG2 promoter methylation during the development of ATLL [5]. Chronic infection of *Helicobacter pylori* in the stomach has been reported to suppress the NDRG2 expression via enhancement of DNMT3β expression with NDRG2 promoter methylation, resulting in promoting gastric cancer progression [39]. Similarly to *Helicobacter pylori* infection, chronic infection of HTLV-1 in T-cells may suppress the NDRG2 expression via enhancement of EZH2 expression through NDRG2 promoter methylation with enhanced H3K27me3 methylation, resulting in promoting ATLL progression. EZH2 and H3K27me3 associated with CpG islands are also reported to induce de novo DNA methylation to silence genes such as ID4 and matrix metalloproteinases through the recruitment of DNMTs in cancer [20,30,40,41]; however, silencing of target genes such as E-cadherin by EZH2-mediated H3K27me3 occurs independently of DNA promoter methylation [42–44]. Since the CpG island of the NDRG2 promoter is highly methylated in ATLL cells, a member of DNMT family may be recruited to the NDRG2 promoter region by EZH2 with H3K27me3. Thus, it is speculated that increased EZH2 expression may be involved in the development of ATLL through the suppression of NDRG2 expression by enhanced promoter methylation.

Dysregulation of EZH2 expression is involved in tumor aggressiveness and metastasis through transcriptional repression of tumor suppressor genes in many types of cancer and is modulated by infection/bacteria, cytokine-induced signal transduction pathways, and microRNAs [45–47]. We showed that EZH2 expression was markedly increased in HTLV-1-infected and ATLL cells and mediated by NF-κB activation. Since there are several potential binding sites for transcription factors such as SRF, Elk1, and STAT1, in the EZH2 promoter region, a detailed study is needed to further clarify the regulation of EZH2 expression in ATLL. Inhibition of EZH2 may prevent the initiation and development of ATLL through the re-activation of tumor suppressor genes, including NDRG2.

Taken together, these findings suggest that while NDRG2 expression is upregulated by HTLV1/Tax-induced NF-κB activity during the early phase of HTLV-1-infection in T-lymphocytes, which could lead to the suppression of aberrant signal transduction pathways, NF-κB-induced EZH2 overexpression inhibits NDRG2 expression through the enhancement of NDRG2 promoter methylation during a long incubation period before the onset of ATLL (Supplementary Fig. 6). Therefore, the expression of NDRG2 and its epigenetic modification may become promising novel targets for cancer diagnosis and therapy.

Transparency document

The Transparency document associated with this article can be found, in online version.

Declaration of Competing Interest

The authors declare no competing interests.

Acknowledgments

We thank Y Motoyoshi, I Morinaga, K Sakamoto and A Nakatake for their technical assistance and Y Yamashita for secretarial assistance. We thank all of the members of the Division of Tumor and Cellular Biochemistry and HTLV-1/ATL Research Facility at the University of Miyazaki for their helpful discussions and comments. Additionally, we gratefully thank all the researchers who kindly provided us with

important cell lines and materials. This study was supported in part by a Grant-in-Aid for Scientific Research (B) (17H03581 to K.M.), Young Scientists (B) (25860242 to T.I.), Scientific Research (C) (18K07238 to T.I.) of Japan Society for the Promotion of Science (JSPS), the Takeda Science Foundation (T.I.), The Tokyo Biochemical Research Foundation (T.I.) and The Shinnihon Foundation of Advanced Medical Treatment Research (T.I.).

Author contributions statement

T.I. and K.M. designed the research. T.I. and S.N. performed the experiments and analyzed the results. M.F. and H.I. provided reagents and materials. K.S. provided patient samples. T.I., S.N. and K.M. wrote the manuscript. K.M. supervised the project.

Appendix A. Supplementary data

Supplementary data to this article can be found online at https://doi.org/10.1016/j.bbadis.2019.07.001.

References

[1] M. Matsuoka, Retrovirology **2** (2005) 27.
[2] M. Yamagishi, T. Watanabe, Front. Microbiol. 3 (2012) 334.
[3] T. Tamura, T. Ichikawa, S. Nakahata, Y. Kondo, Y. Tagawa, K. Yamamoto, K. Nagai, T. Baba, R. Yamaguchi, M. Futakuchi, Y. Yamashita, K. Morishita, Cancer Res. 77 (2017) 2363–2374.
[4] T. Ichikawa, S. Nakahata, M. Fujii, H. Iha, K. Morishita, Sci. Rep. 5 (2015) 12841.
[5] S. Nakahata, T. Ichikawa, P. Maneesaay, Y. Saito, K. Nagai, T. Tamura, N. Manachai, N. Yamakawa, M. Hamasaki, I. Kitabayashi, Y. Arai, Y. Kanai, T. Taki, T. Abe, H. Kiyonari, K. Shimoda, K. Ohshima, A. Horii, H. Shima, M. Taniwaki, R. Yamaguchi, K. Morishita, Nat. Commun. 5 (2014) 3393.
[6] N. Liu, L. Wang, X. Li, Q. Yang, X. Liu, J. Zhang, J. Zhang, Y. Wu, S. Ji, Y. Zhang, A. Yang, H. Han, L. Yao, Nucleic Acids Res. 36 (2008) 5335–5349.
[7] T. Ichikawa, S. Nakahata, T. Tamura, N. Manachai, K. Morishita, Cell. Signal. 27 (2015) 2087–2098.
[8] L. Wang, N. Liu, L. Yao, F. Li, J. Zhang, Y. Deng, J. Liu, S. Ji, A. Yang, H. Han, Y. Zhang, J. Zhang, W. Han, X. Liu, Cell. Physiol. Biochem. 21 (2008) 239–250.
[9] Z.F. Zhang, J. Zhang, Y.N. Hui, M.H. Zheng, X.P. Liu, P.F. Kador, Y.S. Wang, L.B. Yao, J. Zhou, PLoS One 6 (2011) e26102.
[10] K. Takahashi, A. Saitoh, M. Yamada, T. Iwai, M. Inagaki, M. Yamada, J. Neurosci. Res. 90 (2012) 160–166.
[11] T. Li, J. Hu, G.H. He, Y. Li, C.C. Zhu, W.G. Hou, S. Zhang, W. Li, J.S. Zhang, Z. Wang, X.P. Liu, L.B. Yao, Y.Q. Zhang, Biochim. Biophys. Acta 1822 (2012) 301–313.
[12] M. Esteller, Nat. Rev. Genet. 8 (2007) 286–298.
[13] K. Paschos, M.J. Allday, Trends Microbiol. 18 (2010) 439–447.
[14] H. Morimoto, J. Tsukada, Y. Kominato, Y. Tanaka, Am. J. Hematol. 78 (2005) 100–107.
[15] K. Uenogawa, Y. Hatta, N. Arima, S. Hayakawa, U. Sawada, S. Aizawa, T. Yamamoto, J. Takeuchi, Int. J. Mol. Med. 28 (2011) 835–839.
[16] Y. Yang, S. Takeuchi, K. Tsukasaki, Y. Yamada, T. Hata, N. Mori, A. Fukushima, H. Seo, H.P. Koeffler, H. Taguchi, Leuk. Res. 29 (2005) 47–51.
[17] J. Yasunaga, Y. Taniguchi, K. Nosaka, M. Yoshida, Y. Satou, T. Sakai, H. Mitsuya, M. Matsuoka, Cancer Res. 64 (2004) 6002–6009.
[18] A. Chase, N.C. Cross, Clin. Cancer Res. 17 (2011) 2613–2618.
[19] J.A. Simon, C.A. Lange, Mutat. Res. 647 (2008) 21–29.
[20] D. Fujikawa, S. Nakagawa, M. Hori, N. Kurokawa, A. Soejima, K. Nakano, T. Yamochi, M. Nakashima, S. Kobayashi, Y. Tanaka, M. Iwanaga, A. Utsunomiya, K. Uchimaru, M. Yamagishi, T. Watanabe, Blood. 127 (2016) 1790–1802.
[21] D. Sasaki, Y. Imaizumi, H. Hasegawa, A. Osaka, K. Tsukasaki, Y.L. Choi, H. Mano, V.E. Marquez, T. Hayashi, K. Yanagihara, Y. Moriwaki, Y. Miyazaki, S. Kamihira, Y. Yamada, Haematologica. 96 (2011) 712–719.
[22] M. He, W. Zhang, T. Bakken, M. Schutten, Z. Toth, J.U. Jung, P. Gill, M. Cannon, S.J. Gao, Cancer Res. 72 (2012) 3582–3592.
[23] B.C. Roy, D. Subramaniam, I. Ahmed, V.R. Jala, C.M. Hester, K.A. Greiner, B. Haribabu, S. Anant, S. Umar, Oncogene. 34 (2015) 4519–4530.
[24] G.M. De Donatis, E.L. Pape, A. Pierron, Y. Cheli, V. Hofman, P. Hofman, M. Allegra, K. Zahaf, P. Bahadoran, S. Rocchi, C. Bertolotto, R. Ballotti, T. Passeron, Oncogene. 35 (2016) 2735–2745.
[25] A. Iannetti, A.C. Ledoux, S.J. Tudhope, H. Sellier, B. Zhao, S. Mowla, A. Moore, H. Hummerich, B.E. Gewurz, S.J. Cockell, P.S. Jat, E. Willmore, N.D. Perkins, PLoS Genet. 10 (2014) e1004642.
[26] E. Riquelme, C. Behrens, H.Y. Lin, G. Simon, V. Papadimitrakopoulou, J. Izzo, C. Moran, N. Kalhor, J.J. Lee, J.D. Minna, I.I. Wistuba, Cancer Res. 76 (2016) 675–685.
[27] B. Sarkar, I. Nishikata, S. Nakahata, T. Ichikawa, T. Shiraga, H.R. Saha, M. Fujii, Y. Tanaka, K. Shimoda, K. Morishita, Sci. Rep. 9 (2019) 3491.
[28] J. Fujisawa, M. Toita, T. Yoshimura, M. Yoshida, J. Virol. 65 (1991) 4525–4528.
[29] S. Shimosaki, S. Nakahata, T. Ichikawa, A. Kitanaka, T. Kameda, T. Hidaka, Y. Kubuki, G. Kurosawa, L. Zhang, Y. Sudo, K. Shimoda, K. Morishita, Biochem. Biophys. Res. Commun. 485 (2017) 144–151.
[30] Y. Schlesinger, R. Straussman, I. Keshet, S. Farkash, M. Hecht, J. Zimmerman, E. Eden, Z. Yakhini, E. Ben-Shushan, B.E. Reubinoff, Y. Bergman, I. Simon, H. Cedar, Nat. Genet. 39 (2007) 232–236.
[31] H. Takeshima, M. Wakabayashi, N. Hattori, S. Yamashita, T. Ushijima, Carcinogenesis. 36 (2015) 192–201.
[32] S. Fujii, K. Tokita, N. Wada, K. Ito, C. Yamauchi, Y. Ito, A. Ochiai, Oncogene. 30 (2011) 4118–4128.
[33] S. Boulkroun, M. Fay, M.C. Zennaro, B. Escoubet, F. Jaisser, M. Blot-Chabaud, N. Farman, N. Courtois-Coutry, J. Biol. Chem. 277 (2002) 31506–31515.
[34] Y.L. Ma, P. Qin, D.Y. Feng, Y. Li, L.X. Zhang, Z.Y. Liu, A.Q. Yin, W.H. Tang, H.L. Dong, L.Z. Meng, W.G. Hou, L.Z. Xiong, Brain Res. 1569 (2014) 1–8.
[35] X. Chang, Z. Li, J. Ma, P. Deng, S. Zhang, Y. Zhi, J. Chen, D. Dai, Dig. Dis. Sci. 58 (2013) 715–723.
[36] L. Feng, Y. Xie, H. Zhang, Y. Wu, Biochem. Biophys. Res. Commun. 406 (2011) 534–538.
[37] A. Piepoli, R. Cotugno, G. Merla, A. Gentile, B. Augello, M. Quitadamo, A. Merla, A. Panza, M. Carella, R. Maglietta, A. D'Addabbo, N. Ancona, S. Fusilli, F. Perri, A. Andriulli, BMC Med. Genet. 2 (2009) 11.
[38] J. Wang, C. Xie, S. Pan, Y. Liang, J. Han, Y. Lan, J. Sun, K. Li, B. Sun, G. Yang, H. Shi, Y. Li, R. Song, X. Liu, M. Zhu, D. Yin, H. Wang, X. Song, Z. Lu, H. Jiang, T. Zheng, L. Liu, Hepatology. 64 (2016) 1606–1622.
[39] Z.Q. Ling, M.H. Ge, X.X. Lu, J. Han, Y.C. Wu, X. Liu, X. Zhu, L.L. Hong, Oncotarget. 6 (2015) 8210–8225.
[40] S. Chinaranagari, P. Sharma, J. Chaudhary, Oncotarget. 5 (2014) 7172–7182.
[41] Y.J. Shin, J.H. Kim, PLoS One 7 (2012) e30393.
[42] Q. Cao, J. Yu, S.M. Dhanasekaran, J.H. Kim, R.S. Mani, S.A. Tomlins, R. Mehra, B. Laxman, X. Cao, J. Yu, C.G. Kleer, S. Varambally, A.M. Chinnaiyan, Oncogene. 27 (2008) 7274–7284.
[43] S. Fujii, A. Ochiai, Cancer Sci. 99 (2008) 738–746.
[44] Y. Kondo, L. Shen, A.S. Cheng, S. Ahmed, Y. Boumber, C. Charo, T. Yamochi, T. Urano, K. Furukawa, B. Kwabi-Addo, D.L. Gold, Y. Sekido, T.H. Huang, J.P. Issa, Nat. Genet. 40 (2008) 741–750.
[45] Y.F. Lv, G.N. Yan, G. Meng, X. Zhang, Q.N. Guo, Sci. Rep. 5 (2015) 12999.
[46] S. Sander, L. Bullinger, K. Klapproth, K. Fiedler, H.A. Kestler, T.F. Barth, P. Möller, S. Stilgenbauer, J.R. Pollack, T. Wirth, Blood. 112 (2008) 4202–4212.
[47] E. Zhao, T. Maj, I. Kryczek, W. Li, K. Wu, L. Zhao, S. Wei, J. Crespo, S. Wan, L. Vatan, W. Szeliga, I. Shao, Y. Wang, Y. Liu, S. Varambally, A.M. Chinnaiyan, T.H. Welling, V. Marquez, J. Kotarski, H. Wang, Z. Wang, Y. Zhang, R. Liu, G. Wang, W. Zou, Nat. Immunol. 17 (2016) 95–103.